

ELECTRONIC SUPPLEMENTARY INFORMATION

Metal-free boron-doped graphene for selective electroreduction of carbon dioxide to formic acid/formate

Narayanaru Sreekanth^{a†}, Mohammed Nazrulla Azeezulla^{b†}, Thazhe Veetil Vineesh^a, Krishnamurthy Sailaja^{b*}, Kanala Lakshminarasimha Phani^{a*}

^aNanoscale Electrocatalysis Group, Electrodes & Electrocatalysis Division, CSIR-Central Electrochemical Research Institute, Karaikudi-630006, India.

^bFunctional Materials Division, CSIR-Central Electrochemical Research Institute, Karaikudi, 630006, India.

Experimental details

Synthesis of graphene and B doped graphene

Graphene Oxide was prepared by Hummer's method¹, Boron-doped graphene synthesized by using a modification to the method reported in Ref (2). An aliquot of 10 ml solution containing 100 mg boric acid and 20 mg of graphene oxide (5:1 wt ratio) was sonicated for an hour to obtain a uniform mixture. The mixture was dried under vacuum at 80°C. Dried GO – boric acid mixture was ground to a uniform blend and annealed at 900 °C for 4 hours under Ar atmosphere. (B₂O₃ residues are removed by washing with hot water). The product was finally dried under vacuum at 60°C. Graphene was prepared by a similar method by heating GO alone.³

X-ray photoelectron spectroscopy (XPS)

X-ray photoelectron spectroscopy was performed using Thermo Scientific MULTILAB 2000 Base system with Twin Anode Mg/Al (300/400W) X-Ray Source. The deconvoluted high resolution spectrum of B1s in BG shows a peak at 189.4 eV corresponding to BC₃. This indicates that all boron atoms are bonded to the carbon atom in the graphitic plane.²⁻⁴ In addition to BC₃, peaks at other boron-carbon environments such as BC₂O (190.50 eV) and BCO₂ (191.9 eV) are also seen. These signals clearly show that boron atoms are incorporated into the graphene structure. C1s include peak at 284.9 eV (C=C), and peaks at 286.4 eV (C-O), 287.5 eV (C=O), and 288.6 eV (O-C=O) point to different carbon-oxygen bonding²⁻⁴. Atomic percentage of B is approximately 4.1 at%.

Raman spectroscopy

Raman spectroscopy is an effective tool to analyze graphene based materials. Raman spectroscopy of graphene oxide and B- doped graphene was done on a Renishaw Invia Raman Microscope. Raman spectra of graphene oxide and boron-doped graphene show typical D and G bands at 1350 and 1590 cm^{-1} respectively. The I_D/I_G ratio, which is related to the defects in the graphene layer, is low for graphene oxide (0.85) and high for BG (1.05). A high I_D/I_G ratio for BG clearly indicates the existence of many defects in the graphene layers. These defects are due to the doping of B into the hexagonal lattice of C in graphene and also due to the oxidation of graphite.²⁻⁴ Raman spectral results indicate doping of B into graphene layers.

Electrodes

A 3 mm glassy carbon electrode (CH Instruments) and 1 cm^2 glassy carbon plate (Alfa Aeser) were used for the immobilization of B-doped graphene and electrodeposition of Bi. Before catalyst loading, the glassy carbon electrodes were polished using alumina powder (1 μm to 0.05 μm), sonicated and rinsed in ultrapure water. B-doped graphene and graphene inks were prepared by dispersing them in isopropanol (2mg/ ml) and adding 20 μl 5% Nafion[®] solution. A well dispersed ink was drop-cast on the glassy carbon surface and dried overnight. Thin films of Bi were deposited on the glassy carbon surface at -1.1 V vs SCE for a duration of 50 seconds from deoxygenated solutions of 1 mM bismuth nitrate + 5% HNO_3 in 0.1 M acetate buffer.⁵

The Pt UME ($r = 10\mu\text{m}$) was polished using fine alumina powder (0.05 μm) slurry in water, sonicated in Millipore water and then electrochemically polished by cycling in 0.5 M H_2SO_4 solution (potential range: -0.68 to 1V vs MSE). The RG value (ratio of the radius of glass sheath at tip to the radius of Pt wire at the tip) of Pt UME was calculated to be 3 by fitting the approach curve⁶.

Electrochemical measurements

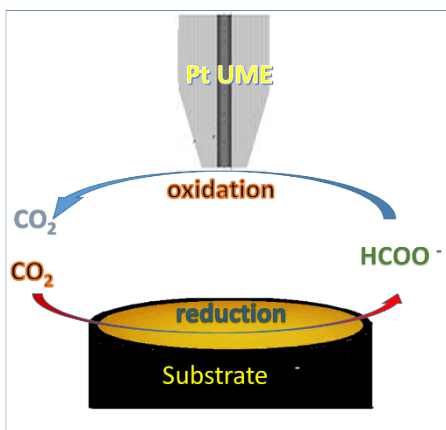
A standard 3-electrode electrochemical cell was used for the LSV and CV measurements using Pt mesh and SCE as counter and reference electrodes respectively. Constant potential electrolysis conducted for quantifying the products was carried out in a two-compartment cell separated by a Nafion[®]-117 membrane. For electrolysis, 0.1M KHCO_3 solution was first bubbled with CO_2 gas for an hour. During electrolysis, a constant flow of CO_2 gas to the cathode compartment was maintained.

The values of the electrochemically active surface area (ECSA) of the boron-doped graphene and graphene were obtained from the voltammetry of a reversible redox, ferrocenemethanol ($\text{Fe}^{2+/3+}$) and the active surface area was calculated using the well-known Randles-Sevcik equation. For finding the ECSA on the Bi electrode, $[\text{Ru}(\text{NH}_3)_6^{2+/3+}]$ redox was employed.⁷ In the case of Pt UME, we used the relationship between the active surface area and the charge under the peaks corresponding to hydrogen adsorption-desorption (hydrogen underpotential deposition).⁸

Scanning electrochemical microscopy

The SECM experiments were conducted by using CHI 900B SECM instrument. SCE and Pt wire served as the reference and counter electrodes respectively for all the experiments. A Pt UME of diameter 10 μm and RG value of 3 was kept at a constant distance of $\approx 10\ \mu\text{m}$ from the substrate using positive feedback mode of SECM in ferrocenemethanol (1 mM) + 0.2 M KCl solutions (Figure S3). After achieving a constant distance between tip and substrate, the solution containing the redox was replaced by the test solution of CO_2 -saturated 0.1 M KHCO_3 .

In the substrate generation-tip collection mode (SG-TC) of SECM, a Pt UME immersed in the same solution opposite the substrate (at a distance of $\approx 10\ \mu\text{m}$) served as the tip electrode for the electro-oxidation of the products of CO_2 reduction at the substrate.⁹ The course of CO_2 reduction was followed at the substrate that is kept at a potential (called substrate potential (E_s)) and the voltammetric patterns were obtained for the oxidation of the species (generated at the substrate) at the Pt UME in a potential region of -0.6V to 1V.



Schematic of SG-TC mode for CO_2 reduction-formate oxidation

Product quantification using NMR Spectroscopy

The liquid-phase products were analyzed qualitatively and quantitatively using ^1H NMR on a Bruker 400MHz NMR instrument. An aliquot of 600 μl electrolyte was taken after two hours of continuous electrolysis for the qualitative analysis. And for the quantification of product an aliquot of 600 μl electrolyte was mixed with 35 μl of 50 mM phenol (for use as an internal standard in D_2O for NMR).¹⁰ The faradaic efficiencies of each product produced were determined from the measured concentration of the product divided by the concentration calculated from the number of coulombs passed during electrolysis.¹¹

$$\text{Faradaic efficiency} = n2F/q$$

where 'n' is number of moles of formate produced, 'F' is Faraday constant and 'q' is number of coulombs passed.

FESEM image and Composition mapping

FESEM characterization was done by using Carl Zeiss SEM instrument (model number: Supra 55VP/41/46) with an accelerating voltage 20 kV using SE or Inlens detector.

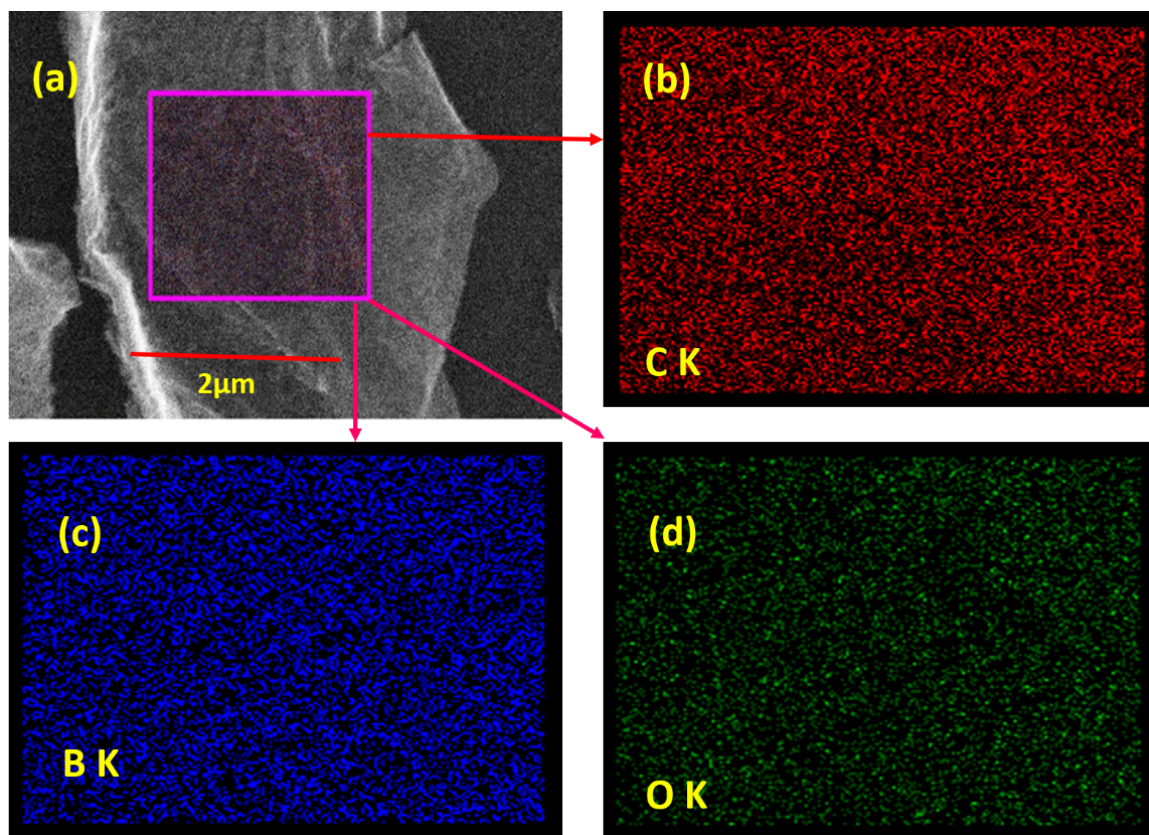


Figure S1: FESEM Image of B-doped graphene (a) and compositional maps for carbon (b), boron (c) and oxygen (d).

TEM Images

TEM characterization was done by using TECHNAI G20 microscope functioning at 200 kV accelerating voltage and samples were prepared on carbon coated copper grid.

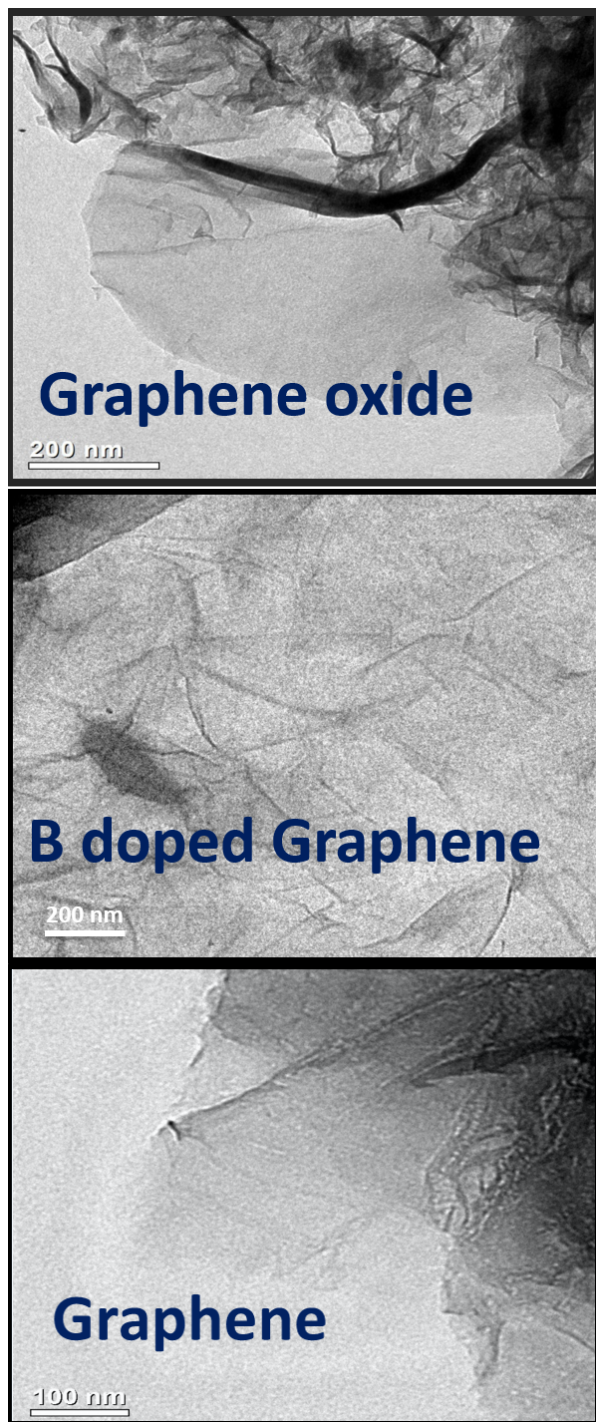


Figure S2: TEM Images of graphene oxide, B-doped graphene and graphene

Obtainment of approach curve for performing SECM

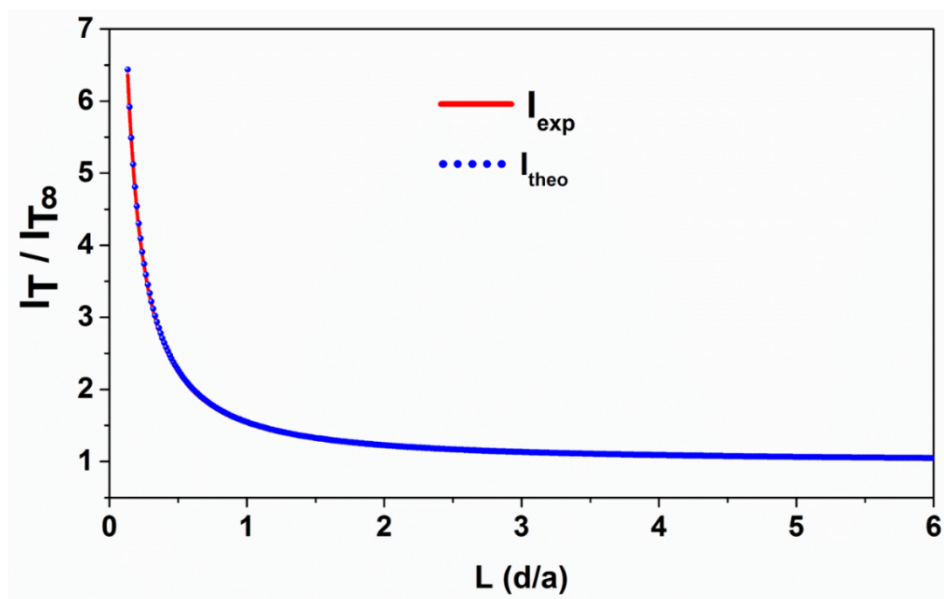


Figure S3: Scanning electrochemical microscopy: experimental and theoretical positive approach curves obtained by taking Pt UME tip (10 μ m) towards B-doped graphene substrate using the response of ferrocenemethanol redox in 0.2M KCl solution.

Identification of CO₂ reduction (electroactive) products using SG-TC mode of SECM

That the reduction process leads solely to the formation of formate is conspicuous by the absence of CV signature responses of CO oxidation at the Pt UME probe. In a control experiment, we show the emergence of CO product during CO₂RR on a gold surface, whose presence is indicated by the typical oxidative voltammetric response of CO oxidation at Pt.

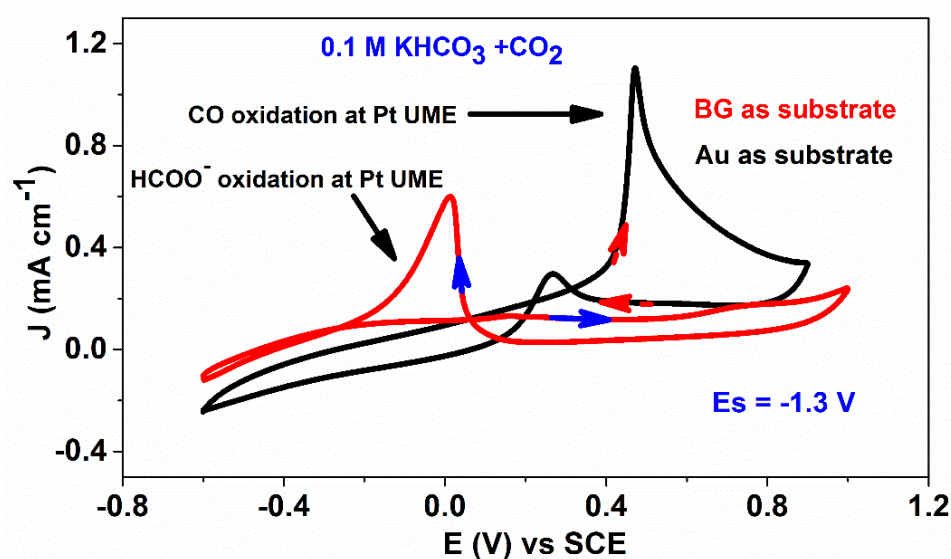


Figure S4: SG-TC Mode: Cyclic voltammetric response of Pt UME tip probe to the product generated from the B doped graphene (red) and Au (black) kept at a substrate potential (E_s) -1.3V in 0.1 M KHCO₃ saturated with CO₂; scan rate 0.05V s⁻¹.

Constant Potential Electrolysis

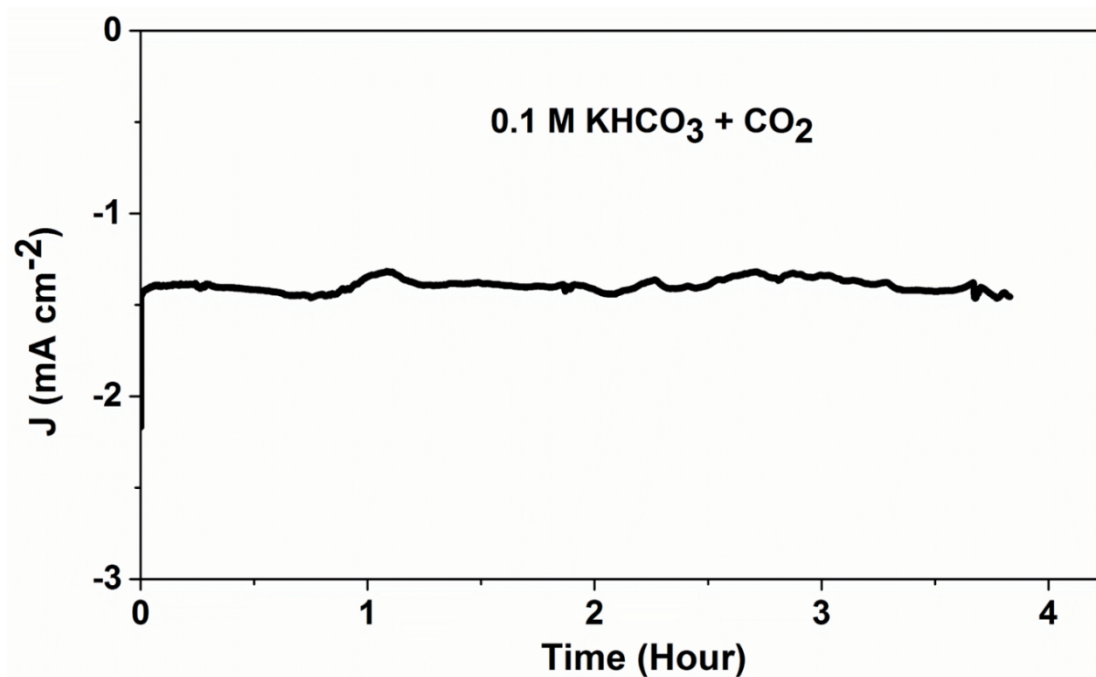


Figure S5: Current –time curve of CO₂ reduction reaction on B doped graphene kept at -1.4V vs SCE in CO₂ saturated 0.1M KHCO₃ solution, for stability measurement and faradaic efficiency calculation

NMR spectra

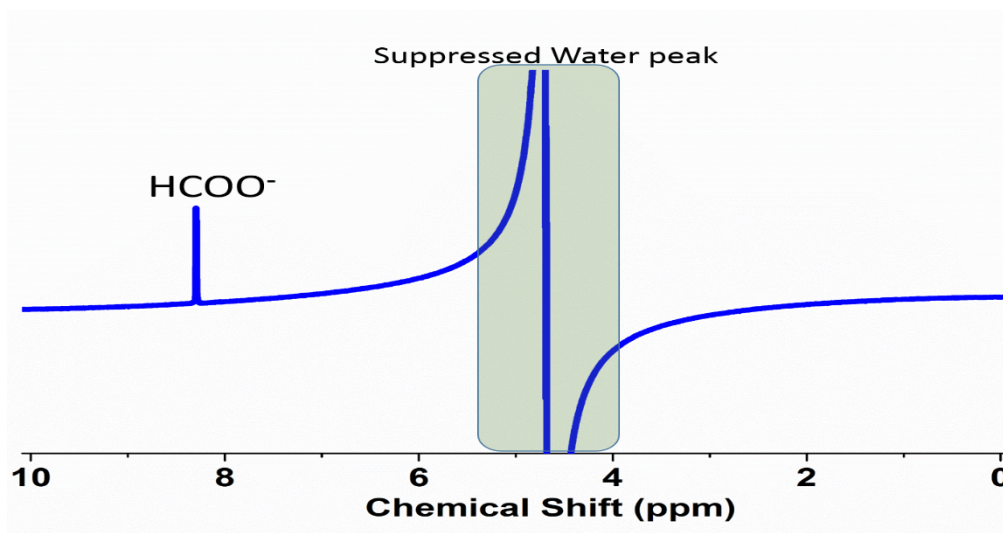


Figure S6: ¹H-NMR spectra of formate obtained after electrolysis of CO₂ saturated 0.1 M KHCO₃ solution on BG surface.

Computational Details

All calculations include spin polarization and are performed within the framework of Density Functional Theory (DFT)^{12, 13} using a linear combination of Gaussian orbitals as implemented in the deMon.2.2.6 code.¹⁴ All the geometries are optimized using the Perdew–Burke–Ernzerhof exchange and correlation functional.¹⁵ The double zeta valence polarization basis set is used for carbon, boron, oxygen, and hydrogen atoms. No additional polarization functions are added. A2 auxiliary functions are added to fit the charge density.¹⁶ The convergence of the geometries is based on the gradient and displacement criteria. Atomic spin and charge densities are based on the Mulliken SCF population analysis.

The adsorption energy (E_{ads}) is calculated as, $E_{\text{ads}} = E_{\text{AB}} - (E_{\text{A}} + E_{\text{B}})$, where E_{AB} is the total energy of the complex (graphene/BG + CO₂, COOH, CO+H₂O, HCOOH) and E_{A} and E_{B} are the individual energies of the graphene/BG and CO₂, COOH, CO+H₂O, HCOOH respectively.

Doping is an efficient way to tune the physico-chemical properties of the materials and introduces asymmetry in the system leading to the asymmetric spin and charge distribution. Atomic spin and charge densities are measures for the catalytic efficacy of the systems towards the oxygen reduction reaction.¹⁷ In order to gain insights and to correlate the experimentally observed results on doped graphene, many researchers have modeled using graphene nanoflakes.^{18, 19} In our calculations, we use a nanodisc-shaped C₄₂H₁₆, a zigzag edged graphene nanoflake (GNF) as a model for graphene. The structure, chemical reactivity and stability of C₄₂H₁₆ can be found elsewhere.²⁰ To this C₄₂H₁₆ GNF, we have doped B atom at various sites (see Table S1) and the ground state geometry of B-doped graphene is designated as C₄₁BH₁₆. Harmonic vibrational frequencies are computed for the ground state geometry and all the frequencies are found to be positive, indicating the optimized geometry as a local minimum.

The graphene and B-graphene models, their frontier molecular orbitals, initial and optimized geometries along with the adsorption energies for CO₂ and COOH are presented in Figures S7 and S8 (Modeling of CO₂ adsorption and reduction phenomena on respectively for pristine graphene and BG).

Formic acid formation against Carbon monoxide over BG

For the completion of the CO₂RR, there is a possibility that a second proton can attack either carbon atom in *COOH or oxygen atom (OH) in *COOH (R1 and R2, in Figure S9 respectively) leading to the formation of two different products in CO₂ reduction, viz., HCOOH (product P1 obtained from reaction R1 and CO (product P2 obtained from reactant R2), as shown in Figure S9. Both R1 and R2 are the localized geometries with a relative energy of $RE_1 = R1 - R2 = -1.01 \text{ kcal mol}^{-1}$ on a potential energy surface. After the reaction, the relative energy between P1 and P2 with respect to R2 is found to be $RE_2 = P1 - P2 = -23.74 \text{ kcal mol}^{-1}$, suggesting a higher probability of formation of formic acid over carbon monoxide. In other words, attack of a second proton on C atom of *COOH is more feasible on BG as compared to its attack on OH of *COOH.

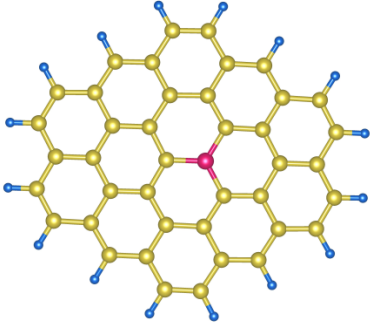
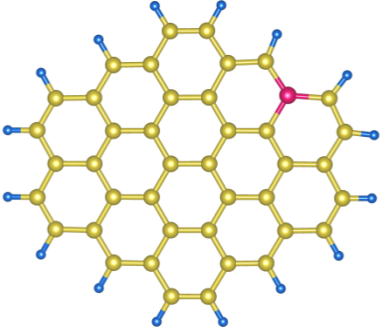
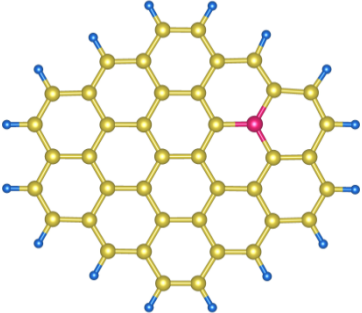
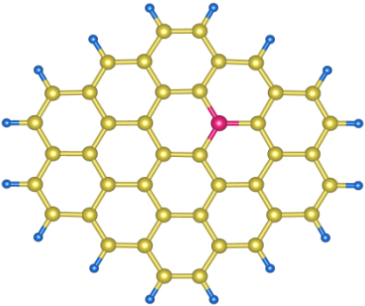
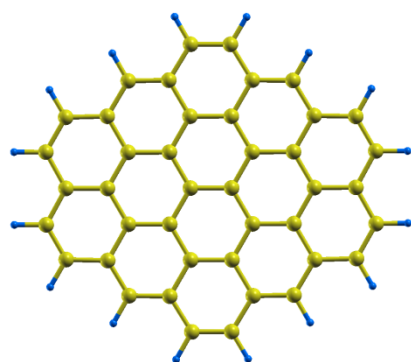
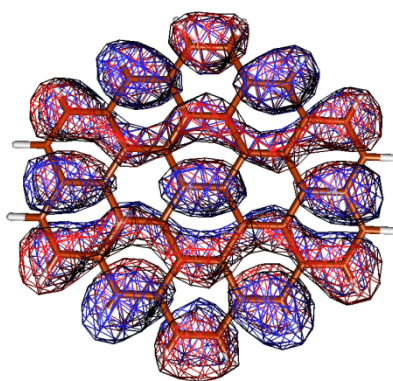
Sl. No.	Boron doping at various sites in Graphene nanoflake	Relative energy (kcal/mol)
1.		0.00 [Ground state geometry- $C_{41}BH_{16}$]
2.		0.10
3.		1.80
4.		3.86

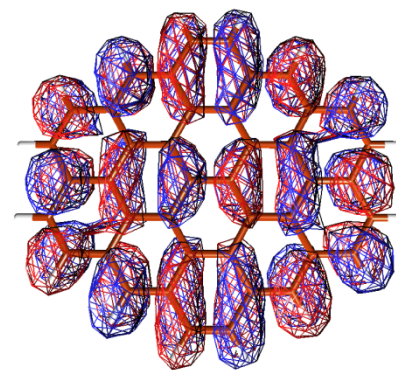
Table S1: various sites for boron doping in graphene nanoflake and their relative energies



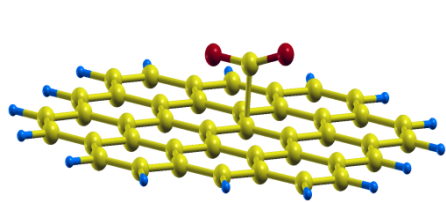
(a) Graphene model ($C_{42}H_{16}$)



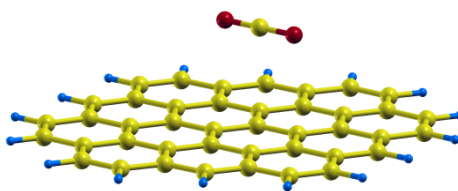
(b) HOMO



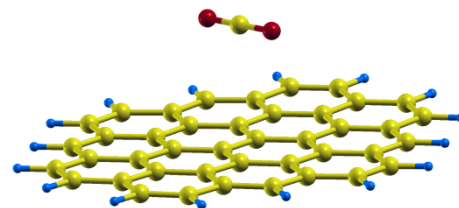
(c) LUMO



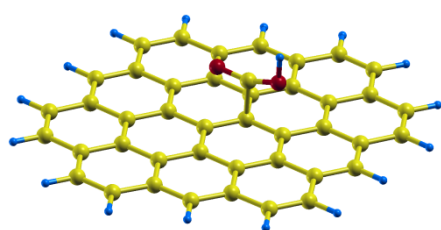
(d) IG1-CO₂



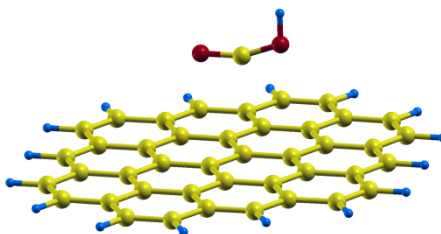
(e) IG2-CO₂



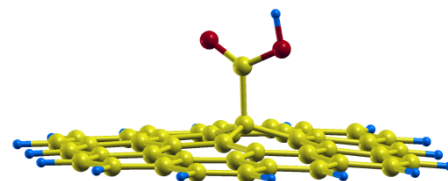
(f) OG-AE = -0.61 kcal/mol



(g) IG1-COOH

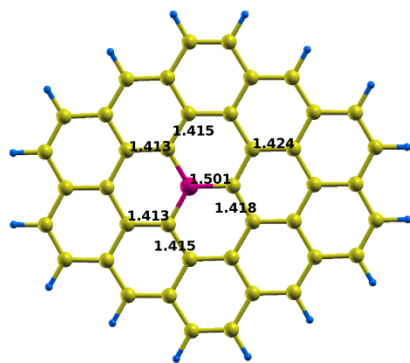


(h) IG2-COOH

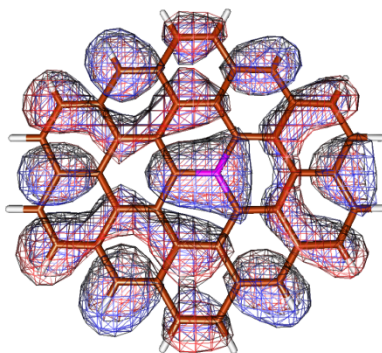


(i) OG-AE = -1.50 kcal/mol

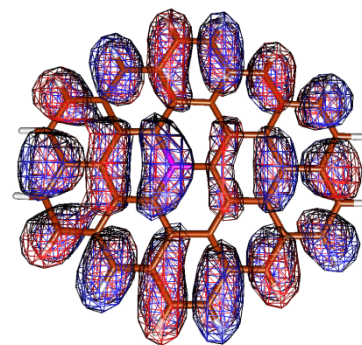
Figure S7: Modeling of CO₂ adsorption and reduction phenomena on pristine graphene: (a) Graphene model ($C_{42}H_{16}$); (b) Highest occupied molecular orbital, HOMO; (c) Lowest unoccupied molecular orbital, LUMO; (d) and (e) Initial geometries (IG1-CO₂ attached to graphene) and IG2-CO₂ at 2 Å far) of CO₂ adsorption on graphene; (f) Optimized geometry (OG) of CO₂ on graphene with its adsorption energy (AE); (g) and (h) Initial geometries (IG1-COOH at 2 Å far) and IG2-COOH attached to graphene) of COOH adsorption on graphene; (i) Optimized geometry (OG) of COOH on graphene with its adsorption energy (AE)



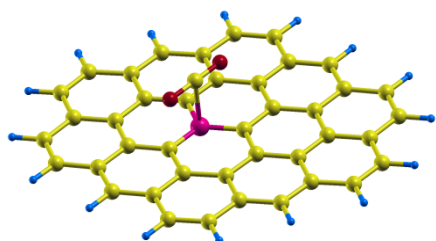
(b) HOMO



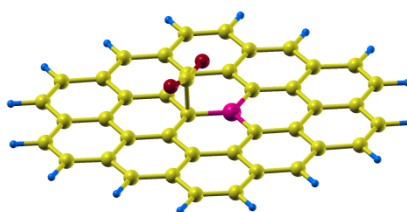
(a) B-doped
(c) LUMO



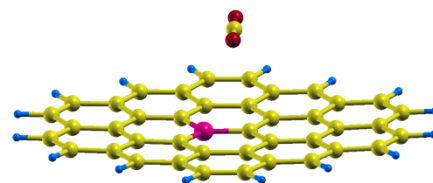
grapheme



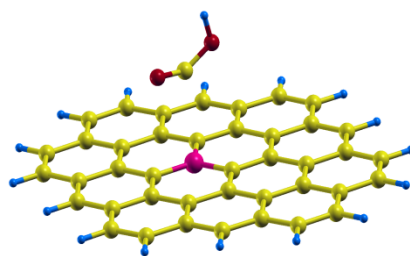
(d) IG1_B-CO₂



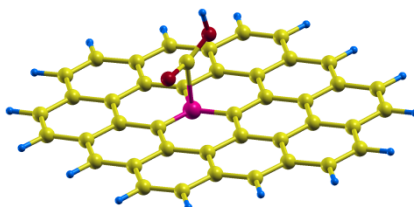
(e) IG2_C-CO₂



(f) OG-AE = -3.40 kcal/mol

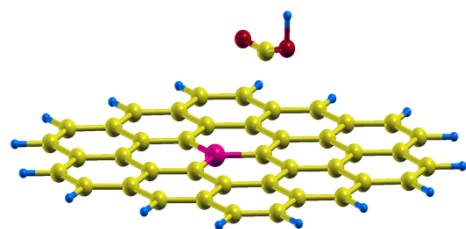
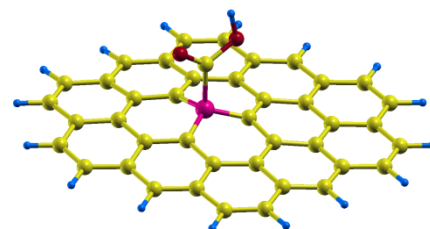


(g) IG1_B-COOH

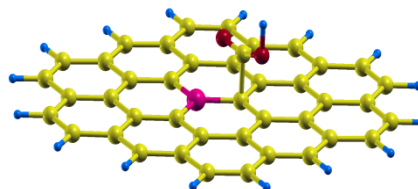


(h) IG2_B-COOH

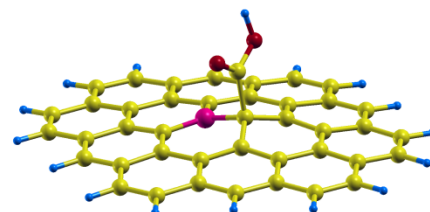
(i) OG-AE = -34.35 kcal/mol



(j) IG1_C-COOH



(k) IG2_C-COOH



(l) OG-AE = -37.55 kcal/mol

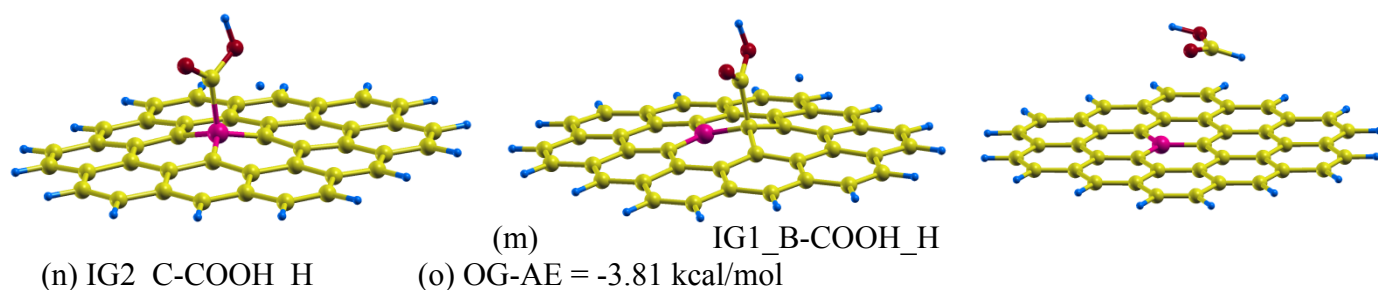


Figure S8: Modeling of CO₂ physisorption and reduction phenomena on boron doped graphene (BG): (a) Boron doped graphene model (C₄₁BH₁₆); (b) Highest occupied molecular orbital, HOMO; (c) Lowest unoccupied molecular orbital, LUMO; (d) and (e) Initial geometries (IG1-CO₂ attached to boron atom in BG and IG2-CO₂ attached to carbon atom in BG) of CO₂ adsorption on BG; (f) Optimized geometry (OG) of CO₂ on BG with its adsorption energy (AE); (g) and (h) Initial geometries (IG1-COOH at 2 Å far over boron atom) and IG2-COOH attached to BG via boron atom) of COOH adsorption on BG through boron atom; (i) Optimized geometry (OG) of COOH on BG through boron atom with its adsorption energy (AE); (j) and (k) Initial geometries (IG1-COOH at 2 Å far over carbon atom) and IG2-COOH attached to BG via carbon atom) of COOH adsorption on BG through carbon atom; (l) Optimized geometry (OG) of COOH on BG through carbon atom with its adsorption energy (AE); (m) and (n) Initial geometries for the attack of second H⁺ for formic acid formation (IG1 and IG2-COOH); (o) Formation of formic acid on BG (optimized geometry (OG) with its adsorption energy).

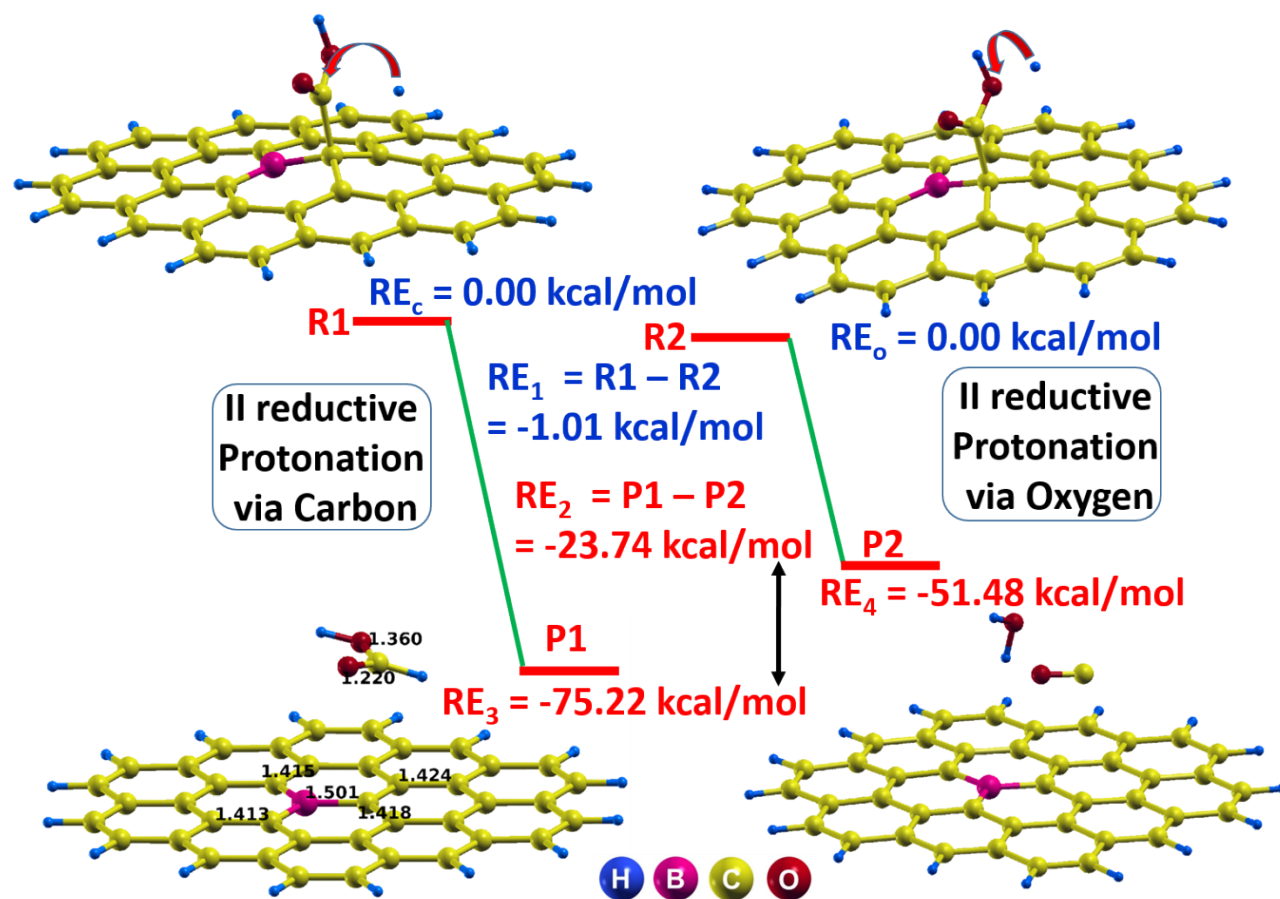


Figure S9: Relative energies (kcal/mol) of reactants; R1 (Attack of H on C of *COOH) and R2 (Attack of H on OH of *COOH) and products; P1 (BG + formic acid) and P2 (BG + CO + H₂O).

References

1. W. S. Hummers, and R.E. Offeman, *J. Am. Chem. Soc.* 1958, **80**, 1339-1339.
2. S. Wang, L. Zhang, Z. Xia, A. Roy, D. W. Chang, J. Baek, and L. Dai, *Angew. Chem. Int. Ed.*, 2012, **51**, 1-5.
3. Z.H.Sheng, H.L.Gao, W.J.Bao, F.B.Wang, and X.H. Xia, *J. Mater. Chem.* 2012, **22**, 390-395.
4. (a) L.S. Panchakarla, K.S. Subrahmanyam, S.K. Saha, A. Govindaraj, H. R. Krishnamurthy, U.V. Waghmare, and C.N.R. Rao, *Adv. Mater.* 2009, **21**, 4726-4730. (b) M. Sahoo, K.P.

- Sreena, B. P. Vinayan, and S. Ramaprabhu, *Mater. Res. Bull.* 2014, **61**, 383-390. (c) Z. Zuo, Z. Jiang and A. Manthiram, *J. Mater. Chem. A*, 2013, **1**, 13476–13483, (d) L. Wang, Z. Sofer, P. Šimek, I. Tomandl, and M. Pumera, *J. Phys. Chem. C* 2013, **117**, 23251–23257
5. J. Wang, J. Lu, S.B. Hocevar, and P.A.M Farias, *Anal. Chem.* 2000, **72**, 3218–3222.
6. M.V. Mirkin, *Scanning Electrochemical Microscopy*, A.J. Bard, and M.V Mirkin, *Marcel Dekker*. 2001, Ch. **5**,145
7. J. L Dimeglio, and J. Rosenthal, *J. Am. Chem. Soc.* 2013, **135**, 8798–8801.
8. S.Trasatti, and O. A. Petrii, *J. Electroanal Chem.*1992, **327**, 353-376.
9. N.Sreekanth, and K. L. N. Phani, *Chem. Commun.*2014, **50**, 11143–11146.
10. K. P.Kuhl, E.R.Cave, D.N.Abram, and T.F.Jaramillo, *Energy Environ. Sci.*2012, **5**, 7050–7059.
11. J.Wu, F.G. Risalvato, F.S. Ke, P.J. Pellechia, and X.D. Zhou, *J. Electrochem. Soc.* 2012, **159**, F353–F359.
12. W.Kohn, and L. Sham, *J. Phys. Rev.* 1965, **137**, A1697-A1705.
13. W.Kohn, and L. Sham, *J. Phys. Rev.* 1965, **140**, A1133-A1138.
14. deMon2k, A.M. Koster, P. Calaminici, M.E. Casida, R.F Moreno, G. Geudtner, A. Goursot, T. Heine, A. Ipatov, F. Janetzko, J.M. Del Campo, S. Patchkovskii, J.U. Reveles, A. Vela, and A.D.R. Salahub, de Mon Developers (2006).
15. J. P. Perdew, K. Burke, and M. Ernzerhof, *Phys. Rev. Lett.* 1996, **77**, 3865.
16. N. Godbout, D.R. Salahub, and J.A.E. Wimmer, *Can. J. Phys.* 1992, **70**, 560.
17. L. Zhang, and Z. Xia, *J. Phys. Chem. C* 2011, **115**, 11170–11176.

18. J. Liang, Y. Jiao, M. Jaroniec, and S.Z. Qiao, *Angew. Chem. Int. Ed.* 2012, **51**, 11496–11500.
19. Y. Zheng, Y. Jiao, L. Ge, M. Jaroniec, and S.Z. Qiao, *Angew. Chemie* 2013, **125**, 3192–3198.
20. M.A. Nazrulla, S. Krishnamurty, and K.L.N. Phani, *J. Phys. Chem. C*. 2014, **118**, 23058–23069.